Nanoscale Advances

ROYAL SOCIETY OF CHEMISTRY

COMMUNICATION

View Article Online
View Journal

Cite this: DOI: 10.1039/d0na00230e

Received 23rd March 2020
Accepted 11th June 2020

DOI: 10.1039/d0na00230e

rsc.li/nanoscale-advances

First-principles study of Na insertion at TiO_2 anatase surfaces: new hints for Na-ion battery design†

Arianna Massaro, [a] Ana B. Muñoz-García, *[b] Pasqualino Maddalena, [b] Federico Bella, [c] Giuseppina Meligrana, [c] Claudio Gerbaldi [c] and Michele Pavone *[a]

Na-ion batteries (NIBs) are attracting widespread interest as a potentially more convenient alternative to current state-of-the-art Li-ion batteries (LIBs), chiefly for large-scale energy storage from renewables. Developing novel active materials is essential for the deployment of NIBs, especially in terms of negative electrodes that can accommodate the larger sodium ions. We focus on TiO_2 anatase, which has been proposed as a promising anode material for the overall balance of performance, stability and cost. As the exposed crystal facets in different morphologies of nanostructured anatase can affect the electrochemical performances, here we report a theoretical investigation of Na^+ adsorption and migration through (101), (100) and (001) surface terminations, thus explaining the different activities toward sodiation reported in the literature. Energy barriers computed by means of the CI-NEB method at the DFT+U level of theory show that the (001) surface is the most effective termination for Na^+ insertion. We also provide a detailed analysis to elucidate that the energy barriers are due to structural modifications of the lattice upon sodiation. From these results we derive new design directions for the development of cheap and effective oxide-based nanostructured electrode materials for advanced NIBs.

Na-ion batteries (NIBs) are at the focus of intense research efforts both in academia and industries.[1,2] The objective is replacing most dominating Li-ion based technologies, because lithium's scarce availability and high costs have hindered their deployment in large-scale storage applications so far.[3–5] On the contrary, thanks to cheap and easily available sodium raw materials, NIB-based devices are foreseen to be a key enabler for the transition to a more sustainable society: from large grid facilities, in combination with renewable energy conversion plants, to even futuristic electric transportation.[6,7] Despite sharing similar operating principles, Li-ion batteries (LIBs) and NIBs sensibly differ in their constituent materials.[8,9] In recent years, the energy storage community attested the resurgence toward rational optimization of various advanced electrode materials. Their thorough design in the form of nanostructures endow the electrodes with high reversible capacity, enhanced rate capability, and prolonged durability.[10] However, the large Na^+ radius helps in the diffusion through liquid electrolytes, but it hampers a convenient Na^+ reversible storage into the structure of the electrodes.[11] While this problem is less relevant for positive electrodes, including layered oxides, phosphate olivines and polyanionic compounds as those exploited in state-of-the-art LIBs,[12] common negative electrodes, *e.g.* graphite or silicon, are not able to reversibly accommodate the larger Na^+ cations.[13] This has motivated the development and optimization of negative electrodes highly effective in NIBs.[14]

Among many proposed systems, titanium dioxide (TiO_2) represents a widely investigated and convenient choice for the overall balance of performance, stability and costs. TiO_2 is a versatile functional material with several applications, ranging from solar cells[15] to photocatalytic water splitting[16] and batteries. In Li^+-based batteries, it showed comparable performances to graphitic materials, such as high reversible theoretical capacity (335 mA h g^{-1}), low volume variation upon cycling (less than 4%) and improved safety, due to the structural robustness and high working potential, but it still suffers from poor electrical conductivity ($\sim$1.9 10^{-12} S m^{-1}) and slow ion diffusion.[17] Combining TiO_2 with conductive materials (*e.g.* graphene, mesoporous carbon, carbon nanotubes, and metal oxides) is effective for enhancing electronic conductivity,[13,18] while nano-engineering is important for favourable diffusion kinetics thanks to short ion diffusion pathways and a large

[a]Department of Chemical Sciences, Università di Napoli Federico II, Comp. Univ. Monte Sant'Angelo, via Cintia 21, 80126 Naples, Italy. E-mail: michele.pavone@unina.it

[b]Department of Physics "Ettore Pancini", Università di Napoli Federico II, Comp. Univ. Monte Sant'Angelo, via Cintia 21, 80126 Naples, Italy. E-mail: anabelen.munozgarcia@unina.it

[c]GAME Lab, Department of Applied Science and Technology, Politecnico di Torino, Corso Duca degli Abruzzi 24, 10129-Torino, Italy

† Electronic supplementary information (ESI) available: structural models, surface energies, oxygen vacancies, higher sodium coverage, CI-NEB results computed at the PBE level of theory, and atomic coordinates for all the intermediates along the Na migration path in each surface. See DOI: 10.1039/d0na00230e

electrode/electrolyte contact area.[19] Recent efforts have been devoted to the development and scale up of nanostructured TiO_2-based materials to be applied as anode materials in lab-scale NIBs.[20–25] Innovative synthetic strategies have been developed aiming at advanced functionalization of TiO_2 nanoparticles (NPs) with carbon coating, thus enhancing the active material performance. Nonetheless, the amount of other components than TiO_2 is rather small and plays no active role.[26] Within this context, the structural features, both in terms of crystallinity and morphology, seem to be crucial in determining the activity of TiO_2 NPs. For example, the work by Longoni *et al.*[24] proves that the performances of anatase NPs as negative electrodes in NIBs depend on the exposed NP surfaces, the (100) and (001) facets being much more effective than the most stable (101) surface. From an atomistic perspective, the behavior of these different surface terminations toward Na^+ uptake remains unclear and there are still open questions about the Na^+ storage mechanism. Actually, to the best of our knowledge, an in-depth understanding of Na–TiO_2 interactions is still missing and a conclusive theoretical interpretation of experimental evidence has not been provided yet. Longoni *et al.*[24] suggest that different exposed surfaces in TiO_2 anatase NPs can act as Na^+-insertion sites. In other terms, beside the expected Na^+ adsorption at NP surfaces, Na^+ insertion can also occur upon cycling, as a result of the pseudocapacitive behavior detected at the electrolyte/electrode interface. Attempts to explain the anatase surface-dependent activities with just the surface adsorption fail in predicting the correct observed trend.[25] In particular, adsorption can only support the experimental evidence regarding the high activity of the (100) surface, but it does not explain the high performances of the NPs exposing the (001) surface. It means that sodium coverage on the surface is not a complete nor reliable model for this electrode/electrolyte interface, where the charge and discharge also involve sodiation/desodiation processes, *i.e.* insertion/deinsertion through the anatase NP lattice.

In an attempt to address this knowledge gap, here we report a thorough first-principles study on Na^+ adsorption and insertion at the (101), (100) and (001) TiO_2 anatase surfaces. Our objective is to decouple the structural and electronic features that drive the interaction between these different anatase NP surface terminations and Na ions, thus proving the mechanism and the origin of the observed selectivity for Na^+ uptake. We first built 6-layer slab models for the (101), (100) and (001) low-index surfaces of TiO_2 anatase and validated our model against experimental and theoretical values from the literature (lattice parameters and surface energies are reported in Tables S1–S3†). We focus on the thermodynamically stable surfaces that have been characterized experimentally and present no significant surface reconstruction in real samples.[24] To avoid fictitious numerical effects, we performed full relaxation of all the atoms in the surface slab models, thus obtaining surface energy values in agreement with the literature (Table S2 and see ref. S2†).

The slab approach is the most commonly adopted method to model NPs. On one hand, crystal surfaces are dominant over the bulk state, due to the high surface/volume ratio in NPs. On the other hand, introducing vacuum space in the extended simulation cell largely reduces the computational cost and the reliability of the model compared to the cluster approaches. The PBE+U minimum-energy structures for the surfaces under study are shown in Fig. S2.† We identified several adsorption and insertion sites as initial structures for our calculations. Insertion sites have been considered both in the subsurface layer (the first one underlying the surface layer) and in the following underlying one, along the [010] Na^+ diffusion channel.[23] For adsorption sites lying on top of the clean surfaces, we chose specific configurations where sodium could then be inserted into the TiO_2 lattice. All the explored configurations converged to a unique structure (see the discussion below). Electronic structure analysis confirms that our model consists of a Na cation interacting with an n-type semiconductor, *e.g.* Na s states appear in the TiO_2 conduction band (*vide infra*).

We calculate both Na adsorption and insertion energies for each surface as follows:

$$E_{ads} = E_{Na_{OUT}} - E_{slab} - \frac{1}{2}E_{Na} \quad (1)$$

$$E_{ins} = E_{Na_{IN}} - E_{slab} - \frac{1}{2}E_{Na} \quad (2)$$

where $E_{Na_{OUT}}$ and $E_{Na_{IN}}$ are the total energies of the optimized slabs with, respectively, one adsorbed and one inserted sodium atom, E_{slab} is the total energy of the clean surface and E_{Na} is the total energy of metallic sodium (2-atoms cell), which is taken as the reference.

In order to explain the different adsorption properties for each surface, we consider that part of the energy variation in this process comes from the distortion energy, *i.e.* the energy required to adapt the TiO_2 lattice in the pristine surface structure to the one in the Na-adsorbed state. We can define this quantity as:

$$E_{dist} = E_{slab}^{Na_{OUT}} - E_{slab}^{slab} \quad (3)$$

where $E_{slab}^{Na_{OUT}}$ and E_{slab}^{slab} are the energies of the slab at the geometry of the Na adsorbed state and in its minimum-energy structure, respectively. Table 1 lists all the energy values computed for the different surface terminations.

Insertion energies slightly differ for ~0.1 eV among each other and from the bulk reference value. The distortion energies calculated for each surface are 0.577, 0.318 and 0.726 eV, for (101), (100) and (001), respectively. From our results, we can say that distortion effects clearly explain the trend in adsorption energies. The highly favourable Na adsorption on the (100)

Table 1 Adsorption, E_{ads}, and insertion, E_{ins}, energies calculated according to eqn (1) and (2), respectively. E_{ins} are compared to the TiO_2 anatase bulk value. E_{dist} is obtained according to eqn (3). The reported values are computed at the PBE+U level of theory

	E_{ads} (eV)	E_{ins} (eV)	E_{dist} (eV)
Bulk		0.531	
(101)	−1.120	0.266	0.577
(100)	−1.554	0.460	0.318
(001)	−0.801	0.364	0.726

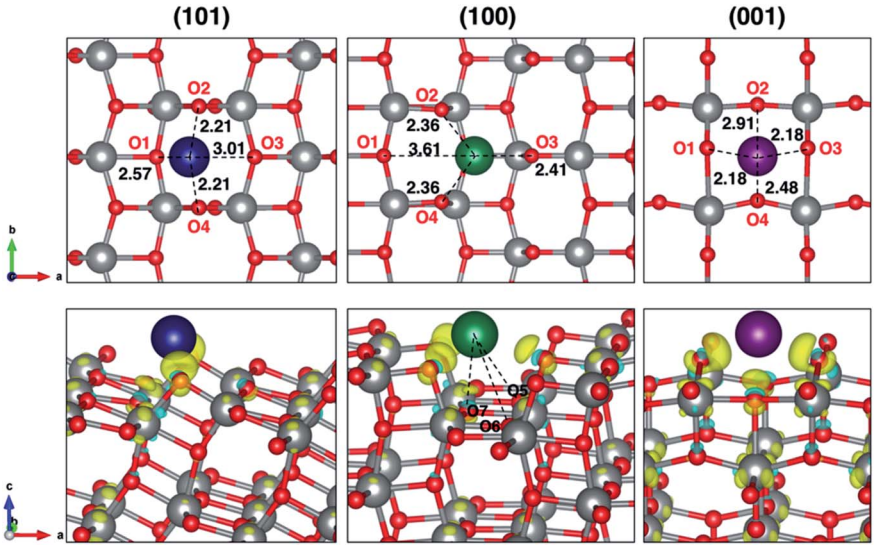

Fig. 1 Top-view projection of the minimum-energy structures for Na_1 adsorbed on the TiO_2 surface slabs with Na–O distances expressed in Å (top panel) and corresponding charge–density difference plots (bottom panel), isodensity value 0.004 a.u. The yellow surface represents electron gain, whereas the blue surface represents electron loss. Ti atoms are depicted in grey, O in red, Na in blue, green and purple, respectively, for (101), (100) and (001) surfaces. Na–O extra interactions are highlighted in the (100) adsorption site (Na–O5 and Na–O6 are 3.51 Å and Na–O7 is 2.59 Å).

surface is also supported by three extra Na–O interactions that are peculiar on this adsorption site, as shown in Fig. 1. Further structural modifications (*e.g.* phase transition) are likely to be less significant when anatase is synthesized in the form of NPs.[27] Indeed, the high surface/volume ratio of the NPs allows sodium to intercalate at most to the subsurface layer. Thus, the full sodiation limit is not reached. However, we addressed eventual structural effects on the subsequent insertion of another Na ion, which actually did not reveal any difference in adsorption and insertion properties.

Electronic structure analysis by charge difference plots (Fig. 1, bottom panel) and PDOS (Fig. 2) show a common pattern for all the surface terminations. The adsorption of a Na atom leads to the reduction of Ti species and population of states at the edge of the TiO_2 conduction band, which is consistent with the desired n-type conductivity for the NIB electrode. At the same time, there is a consistent polarization of the oxygen species that coordinate the adsorbed Na cations, determining the different relative stabilities of the resulting systems.

Besides the adsorption process, Na^+ insertion at the subsurface level is very likely to occur in TiO_2 anatase NPs. Thus, we considered the minimum-energy structures of Na-adsorbed (Na_{OUT}) and Na-inserted (Na_{IN}) systems as the initial and final equilibrium states, respectively, along the process coordinate, *i.e.* the migration path. We applied the climbing image-nudge elastic band (CI-NEB)[28] method to compute the minimum energy path (MEP) between the two states of interest,

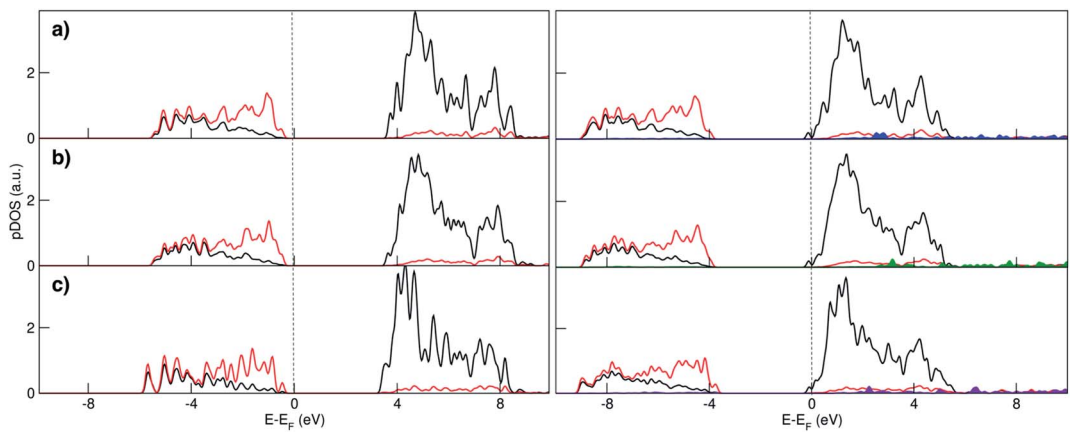

Fig. 2 Atom- and angular momentum- projected density of states for the (a) (101), (b) (100) and (c) (001) TiO_2 surface slabs before (left panel) and after Na adsorption (right panel) at the HSE06 level of theory. Black lines represent Ti d states, red lines O p states, while Na s states are reported in blue, green and violet respectively for (101), (100) and (001) surfaces.

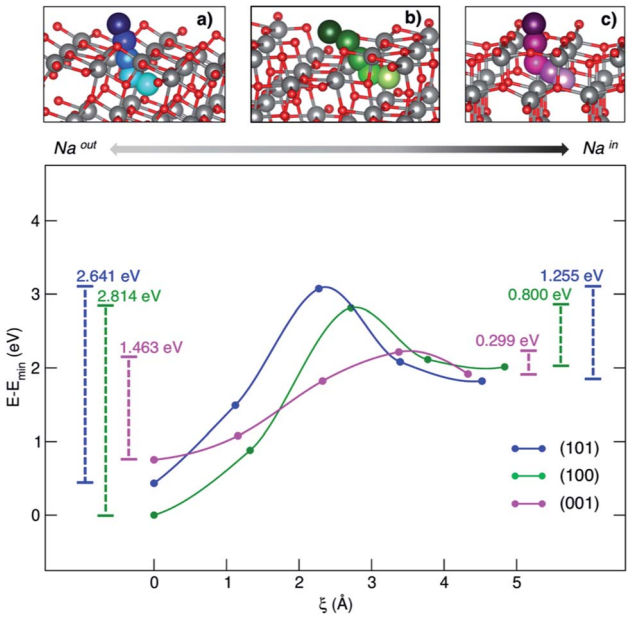

Fig. 3 MEP (top panel) and corresponding energetics (bottom panel) for the Na-migration through the (a) (101), (b) (100) and (c) (001) surfaces. Energy barriers calculated from eqn (4) and (5) for the out/in migration are reported, respectively, at the left- and right-hand sides of the graph.

Na_{OUT} and Na_{IN}, respectively. We modelled the path of Na from surface to the subsurface positions through three intermediate structures (images) that are optimized at the PBE+U level of theory according to the CI-NEB approach. Fig. 3 shows the pictorial representation of the so-obtained MEPs for each surface and their corresponding relative energies.

The process coordinate, ξ, is defined as the Na–Na distance between two contiguous points. The computed MEPs are identical in both forward and backward processes, *i.e.* sodiation/desodiation.

The anatase phase shows a 3D network formed by the stacking of zigzag chains, which consist of distorted edge-sharing TiO_6 octahedra. In this crystal framework, empty channels are possible interstitial sites for ion insertion and suitable-sized pathways for ion diffusion. As it can be observed in the top panel of Fig. 3, sodium moves along a given direction in the lattice, passes across the alternating Ti–O motif, that we will call the "lattice window" from this point forward, and then enters the cavity in the subsurface layer. The cavity lies on the [010] diffusion channel. The coordinates of the computed MEPs are given in the ESI.† The energy barriers associated with both sodiation and desodiation processes can be determined as:

$$E_{migr}^{OUT} = E_{Na_{TS}} - E_{Na_{OUT}} \quad (4)$$

$$E_{migr}^{IN} = E_{Na_{IN}} - E_{Na_{TS}} \quad (5)$$

where $E_{Na_{OUT}}$, $E_{Na_{TS}}$ and $E_{Na_{IN}}$ are the total energies of the initial, transition, and final states, respectively, along the MEP. The calculated E_{migr} for the in/out process are showed in Fig. 3 (bottom panel). We get the lowest energy barrier in both sodiation/desodiation directions for the (001) surface, which means that Na-migration through the (001) crystal facet is much more probable than in the case of (100) and (101) terminations. Since PBE+U provided slightly extended lattice constants with respect to experimental ones (3.5% error), we also performed the same CI-NEB calculations at the PBE level of theory, which provided a closer agreement with experimental structures (only ~2% max error); see results in Fig. S3 of the ESI.† PBE and PBE+U results are qualitatively consistent, confirming the trend for computed barrier heights with (101) > (100) > (001).

The positive values reported so far (insertion and migration energies) are consistent with the non-spontaneous sodiation of TiO_2 anatase NPs. Our model is a reliable representation of an anode interface that can only be sodiated upon charge (*i.e.* provided an electrical potential is supplied). The inclusion in our model of other elements that in principle may lower these

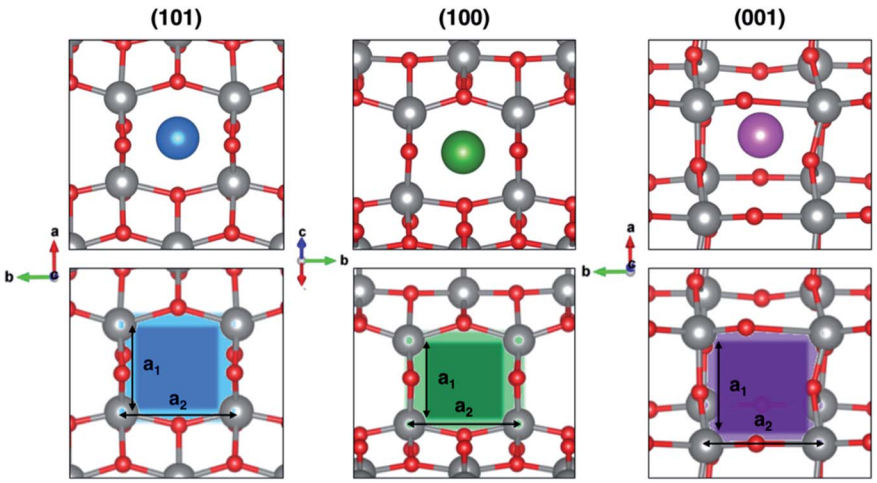

Fig. 4 Top-view projection of the highest-energy structures along the migration path, Na_{TS}, for each surface (top panel) and the corresponding lattice windows (bottom panel). Color code: Ti atoms in grey, O in red, Na in blue, green and purple in (101), (100) and (001) surfaces, respectively.

Table 2 Total (A_{tot}) and minimum accessible (a_{min}) areas of the lattice windows as shown in Fig. 4. Na_{OUT} refers to the minimum-energy structure of the adsorbed Na ions (Fig. 1) and Na_{TS} to that of the transition state structure (Fig. 4)

	A_{tot} (Å^2)		a_{min} (Å^2)		
	Na_{OUT}	Na_{TS}	Na_{OUT}	Na_{TS}	E_{migr}^{OUT} (eV)
(101)	11.4	12.3	8.7	9.6	2.641
(100)	11.4	12.6	8.7	9.9	2.814
(001)	15.2	14.9	15.1	14.8	1.463

values, such as the presence of an electrolyte at the electrode interface and the resulting passivating layer that can be formed or an external applied potential, is beyond the aim of this work. Our purpose is to provide the simplest theoretical model that is able to explain the surface activities reported experimentally.

In order to rationalize such a trend, we focus on the structural features of the different surface terminations. We find that the size of the lattice window at the transition state (Na_{TS}) provides a direct measure of the steric hindrance that the migrating sodium encounters along its path. As highlighted in Fig. 4, the lattice window is the area delimited by the Ti–O lattice and perpendicular to the path that the migrating sodium should cross in order to enter the TiO_2 crystalline structure.

The total area (A) of the lattice window for each surface can be calculated straightforwardly from two Ti–Ti distances, a_1 and a_2. However, this descriptor does not capture the significant difference between the lowest barrier found in (001) and the two higher ones in (100) and (101), as it can be seen from Table 2. Indeed, the limiting factor in the sodium path is related to an "effective" lattice window, which is delimited by the shortest Ti–Ti distance, a_1, thus defining the minimum accessible area, a_{min}.

The minimum accessible area (a_{min}) indirectly correlates with the migration barrier heights calculated for the different surfaces. In fact, smaller lattice windows in (101) and (100) surfaces result in higher barriers, while the (001) surface shows the largest lattice window and, thus, the lowest barrier.

In conclusion, our results show for TiO_2 anatase surfaces the most favourable adsorption of Na^+ at the (100) termination, thanks to a convenient accommodation of the large cations on a surface step that maximizes the Na^+–O^{2-} interactions and does not disturb much the crystalline lattice. Moreover, we find that charge/discharge processes in TiO_2 anatase NPs can effectively occur *via* the Na-insertion mechanism, and we prove that the (001) surface is the most active toward Na subsurface insertion thanks to its peculiar structural features: the large surface lattice window allows for an easy diffusion of the large sodium cations, thus supporting the experimental observation of high performances in NIBs with TiO_2 NPs exposing the (001) surface termination. Analysis of MEPs in all the surface terminations demonstrates that the corresponding migration barrier heights depend only on structural modification of the anatase lattice upon Na^+ insertion, thus unveiling the key role of surface lattice windows. The identification of this easy computable structural description can be very useful and, actually, instrumental for the rational design and development of new, high-performance materials with a potential efficient Na uptake mechanism, particularly nanostructured oxide-based materials having promising Na-host characteristics in NIBs. Our future work will pursue this direction, extending the modelling approaches that are able to correctly reproduce the capacity–voltage profiles of promising electrode materials and also focusing on the interfacial effects induced by dopants or additives, such as C-based materials and nanostructure engineering on the Na-insertion process in anatase-based anodes for NIB applications.

Methods and computational details

Spin-polarized density functional theory (DFT)[29]+U theory[30] was employed to overcome the large self-interaction error that affects DFT when applied to mid-to-late first row transition metal oxides with tightly localized d-electrons. Our calculations were performed with projector-augmented wave (PAW) potentials and plane wave (PW) basis sets, as implemented in the Vienna *ab initio* simulation package (VASP) code (version 5.4.1).[31] We used the Perdew–Burke–Ernzerhof (PBE)[32] exchange-correlation functional with the U_{eff} = 3.3 eV parameter for Ti atoms[33] and the standard PAW potentials. A kinetic energy of 600 eV was used to converge the PW basis set.

Our surface models consist of 6-layer slabs containing 24 formula units (72 atoms). We used 2 × 2 × 1 k-point sampling based on the Monkhorst–Pack scheme. We employ the CI-NEB[28] to locate minimum energy paths of Na migration from the surface to the subsurface and to compute the corresponding barrier heights. We also performed some preliminary tests on smaller cells (36 atoms, 12 f.u.) in order to model a larger sodium coverage, but no change in the observed energetics was detected (Table S6†). However, the 36 atoms-containing cells were rather too small to accommodate all the intermediate structures along Na^+ migration paths, thus we needed to build up supercells in order to perform NEB calculations. Both the minimum-energy and intermediate structures have been obtained through relaxation of all layers in the slab. The projected density of states plots are computed *via* single-point energy calculations at the HSE06 level of theory[34,35] on the PBE+U minimum-energy structures. All the results reported in the manuscript refer to perfect surfaces, although a brief discussion on adsorption and insertion energetics in reduced anatase can be found in the ESI.†

Conflicts of interest

There are no conflicts of interest to declare.

Acknowledgements

MP acknowledges funding from the Italian Ministry of University and Research (MIUR) under grant PRIN 2015XBZ5YA. Authors acknowledge the European Union (FSE, PON Ricerca e Innovazione 2014–2020, Azione I.1 "Dottorati Innovativi con

caratterizzazione Industriale"), for funding a PhD grant to Arianna Massaro. Part of this work was carried out within the activities "Ricerca Sistema Elettrico" funded through contributions to research and development by the Italian Ministry of Economic Development. The computing resources and the related technical support used for this work have been provided by CRESCO/ENEAGRID High Performance Computing infrastructure and its staff;[36] CRESCO/ENEAGRID High Performance Computing infrastructure is funded by ENEA, the Italian National Agency for New Technologies, Energy and Sustainable Economic Development and by Italian and European research programmes. See: http://www.cresco.enea.it/english for information.

References

1 K. Kubota and S. Komaba, Review - Practical Issues and Future Perspective for Na-Ion Batteries, *J. Electrochem. Soc.*, 2015, **162**, A2538–A2550.
2 C. Delmas, Sodium and Sodium-Ion Batteries: 50 Years of Research, *Adv. Energy Mater.*, 2018, **8**, 1703137.
3 J. M. Tarascon, Is lithium the new gold?, *Nat. Chem.*, 2010, **2**, 510.
4 C. Vaalma, D. Buchholz, M. Weil and S. Passerini, A cost and resource analysis of sodium-ion batteries, *Nat. Rev. Mater.*, 2018, **3**, 18013.
5 A. Ponrouch and M. Rosa Palacín, Post-Li batteries: promises and challenges, *Philos. Trans. R. Soc., A*, 2019, **377**, 20180297.
6 D. Larcher and J. M. Tarascon, Towards Greener and More Sustainable Batteries for Electrical Energy Storage, *Nat. Chem.*, 2015, **7**, 19–29.
7 G. Yan, S. Mariyappan, G. Rousse, Q. Jacquet, M. Deschamps, R. David, B. Mirvaux, J. W. Freeland and J.-M. Tarascon, Higher energy and safer sodium ion batteries *via* an electrochemically made disordered $Na_3V_2(PO_4)_2F_3$ material, *Nat. Commun.*, 2019, **10**, 585.
8 K. Chayambuka, G. Mulder, D. L. Danilov and P. H. L. Notten, Sodium-Ion Battery Materials and Electrochemical Properties Reviewed, *Adv. Energy Mater.*, 2018, **8**, 1800079.
9 Y. Huang, Y. Zheng, X. Li, F. Adams, W. Luo, Y. Huang and L. Hu, Electrode Materials of Sodium-Ion Batteries toward Practical Application, *ACS Energy Lett.*, 2018, **3**, 1604–1612.
10 Y. Fang, X.-Y. Yu and X. W. Lou, Nanostructured Electrode Materials for Advanced Sodium-Ion Batteries, *Matter*, 2019, **1**, 90–114.
11 L. P. Wang, L. Yu, X. Wang, M. Srinivasan and Z. J. Xu, Recent Developments in Electrode Materials for Sodium-Ion Batteries, *J. Mater. Chem. A*, 2015, **3**, 9353–9378.
12 Z. Dai, U. Mani, H. Teng Tan and Q. Yan, Advanced Cathode Materials for Sodium-Ion Batteries: What Determines Our Choices?, *Small Methods*, 2017, **1**, 1700098–1700124.
13 Y. Lu, Y. Lu, Z. Niu and J. Chen, Graphene-Based Nanomaterials for Sodium-Ion Batteries, *Adv. Energy Mater.*, 2018, 1702469.
14 L. Li, Y. Zheng, S. Zhang, J. Yang, Z. Shao and Z. Guo, Recent progress on sodium ion batteries: Potential high-performance anodes, *Energy Environ. Sci.*, 2018, **11**, 2310–2340.
15 A. Hagfeldt, G. Boschloo, L. Sun, L. Kloo and H. Pettersson, Dye-Sensitized Solar Cells, *Chem. Rev.*, 2010, **110**, 6595–6663.
16 M. Ni, M. K. H. Leung, D. Y. C. Leung and K. Sumathy, A Review and Recent Developments in Photocatalytic Water-Splitting Using TiO_2 Or Hydrogen Production, *Renewable Sustainable Energy Rev.*, 2007, **11**, 401–425.
17 C. Jiang and J. Zhang, Nanoengineering Titania for High Rate Lithium Storage: A Review, *J. Mater. Sci. Technol.*, 2013, **29**(2), 97–122.
18 Y. C. Yang, B. Qiao, X. Yang, L. Fang, C. Pan, W. Song, H. Hou and X. Ji, Lithium Titanate Tailored by Cathodically Induced Graphene for an Ultrafast Lithium Ion Battery, *Adv. Funct. Mater.*, 2014, **24**, 4349–4356.
19 P. G. Bruce, B. Scrosati and J. M. Tarascon, Nanomaterials for Rechargeable Lithium Batteries, *Angew. Chem., Int. Ed.*, 2008, **47**, 2930–2946.
20 Y. Xu, E. M. Lotfabad, H. Wang, B. Farbod, Z. Xu, A. Kohandehghan and D. Mitlin, Nanocrystalline Anatase TiO_2: A New Anode Material for Rechargeable Sodium Ion Batteries, *Chem. Commun.*, 2013, **49**, 8973–8975.
21 H. Xiong, M. D. Slater, M. Balasubramanian, C. S. Johnson and T. Rajh, Amorphous TiO_2 Nanotube Anode for Rechargeable Sodium Ion Batteries, *J. Phys. Chem. Lett.*, 2011, **2**, 2560–2565.
22 Y. Liu, F. Zhao, J. Li, L. Yanguang, J. A. McLeod and L. Liu, Influence of Crystal Phase on TiO_2 Nanowire Anodes in Sodium Ion Batteries, *J. Mater. Chem. A*, 2017, **5**, 20005–20013.
23 F. Bella, A. B. Muñoz-Garcìa, G. Meligrana, A. Lamberti, M. Destro, M. Pavone and C. Gerbaldi, Unveiling the Controversial Mechanism of Reversible Na Storage in TiO_2 Nanotube Arrays: Amorphous *versus* Anatase TiO_2, *Nano Res.*, 2017, **10**(8), 2891–2903.
24 G. Longoni, R. L. Pena Cabrera, S. Polizzi, M. D'Arienzo, C. M. Mari, Y. Cui and R. Ruffo, Shape-Controlled TiO_2 Nanocrystals for Na-ion Battery Electrodes: The Role of Different Exposed Crystal Facets on the Electrochemical Properties, *Nano Lett.*, 2017, **17**, 992–1000.
25 X. Yang, C. Wang, Y. Yang, Y. Zhang, X. Jia, J. Chen and X. Ji, Anatase TiO_2 Nanocubes for Fast and Durable Sodium Ion Battery Anodes, *J. Mater. Chem. A*, 2015, **3**, 8800–8807.
26 M. N. Tahir, B. Oschmann, D. Buchholz, X. Dou, I. Lieberwirth, M. Panthöfer, W. Tremel, R. Zentel and S. Passerini, Extraordinary Performance of Carbon-Coated Anatase TiO_2 as Sodium-Ion Anode, *Adv. Energy Mater.*, 2016, **6**, 1501489.
27 W. Li, M. Fukunishi, B. J. Morgan, O. J. Borkiewicz, K. W. Chapman, V. Pralong, A. Maignan, O. I. Lebedev, J. Ma, H. Groult, S. Komaba and D. Dambournet, A Reversible Phase Transition for Sodium Insertion in Anatase TiO_2, *Chem. Mater.*, 2017, **29**(4), 1836–1844.
28 G. Henkelman, B. P. Uberuagua and H. Jonsson, A Climbing Image Nudged Elastic Band Method for Finding Saddle Points and Minimum Energy Paths, *J. Chem. Phys.*, 2000, **22**, 113.

29 P. Hohenberg and W. Kohn, Inhomogeneous Electron Gas, *Phys. Rev.*, 1964, **136**, B864; W. Kohn and L. J. Sham, Self-Consistent Equation Including Exchange and Correlation Effects, *Phys. Rev.*, 1965, **140**, A1133.

30 V. I. Anisimov, J. Zaanen and O. K. Andersen, Band theory and Mott Insulators: Hubbard *U* instead of Stoner *I*, *Phys. Rev. B*, 1991, **44**, 943.

31 G. Kresse and J. Furthmüller, Efficient Iterative Schemes for *Ab Initio* Total-Energy Calculations Using A Plane-Wave Basis Set, *Phys. Rev. B: Condens. Matter Mater. Phys.*, 1996, **54**, 11169.

32 J. P. Perdew, K. Burke and M. Ernzerhof, Generalized Gradient Approximation Made Simple, *Phys. Rev. Lett.*, 1996, **77**, 3865.

33 E. Finazzi, C. Di Valentin, G. Pacchioni and A. Selloni, Excess Electron States in Reduced Bulk Anatase TiO_2: Comparison of Standard GGA, GGA+*U* and Hybrid DFT Calculations, *J. Chem. Phys.*, 2008, **129**, 154113.

34 J. Heyd, G. E. Scuseria and M. Ernzerhof, Hybrid functionals based on a screened Coulomb potential, *J. Chem. Phys.*, 2003, **118**, 8207–8215.

35 J. Heyd, G. E. Scuseria and M. Ernzerhof, Erratum: hybrid functionals based on a screened Coulomb potential, *J. Chem. Phys.*, 2003, **118**, 8207; *J. Chem. Phys.*, 2006, **124**, 219906.

36 G. Ponti; F. Palombi; D. Abate; F. Ambrosino; G. Aprea; T. Bastianelli; F. Beone; R. Bertini; G. Bracco; M. Caporicci; B. Calosso; M. Chinnici; A. Colavincenzo; A. Cucurullo; P. Dangelo; M. D. Rosa; P. D. Michele; A. Funel; G. Furini; D. Giammattei; S. Giusepponi; R. Guadagni; G. Guarnieri; A. Italiano; S. Magagnino; A. Mariano; G. Mencuccini; C. Mercuri; S. Migliori; P. Ornelli; S. Pecoraro; A. Perozziello; S. Pierattini; S. Podda; F. Poggi; A. Quintiliani; A. Rocchi; C. Scio; F. Simoni and A. Vita The role of medium size facilities in the HPC ecosystem: the case of the new CRESCO4 cluster integrated in the ENEAGRID infrastructure, *International Conference on High Performance Computing & Simulation* (HPCS), 2014, pp. 1030–1033.